J|A|C|S COMMUNICATIONS

Published on Web 06/11/2010

Phosphine-Free Synthesis of p-Type Copper(I) Selenide Nanocrystals in Hot Coordinating Solvents

Sasanka Deka,[†] Alessandro Genovese,[†] Yang Zhang,[†] Karol Miszta,[†] Giovanni Bertoni,[†] Roman Krahne,[†] Cinzia Giannini,[‡] and Liberato Manna*[,†]

Istituto Italiano di Tecnologia, Via Morego 30, 16163 Genova, Italy, and CNR-Istituto di Crystallografia (IC), Via Amendola 122/O, I-70126 Bari, Italy

Received April 16, 2010; E-mail: liberato.manna@iit.it

The fabrication of low-cost, efficient solar cells made of green materials is a main goal of energy-related research.[1] Several copper-based materials, such as Cu_2S, $CuInS_2$, $CuInSe_2$, $CuIn_xGa_{1-x}Se_2$, and Cu_2ZnSnS_4, have been explored to date in photovoltaics, mainly as thin films,[2] but recently, colloidal nanocrystals of these materials have also been developed and used to make solar cells.[3] Today "all-nanocrystal" or organic−inorganic nanocomposite films can be prepared over large areas using various deposition techniques. Also, copper selenide, a superionic conductor, has been studied in thin-film applications in photovoltaics, optical filters, and dry galvanic cells (as a solid electrolyte).[1e,2c] It can form in many stoichiometries (Cu_2Se, $Cu_{2-x}Se$, $CuSe$, Cu_2Se_3) and phases. Copper(I) selenide (Cu_2Se, $Cu_{2-x}Se$) crystallizes generally in the face-centered cubic berzelianite phase.[4] $Cu_{2-x}Se$ has both a direct band gap of 2.2 eV and an indirect band gap of 1.4 eV (at the limit for solar cell applications) and shows p-type conductivity. Nanocrystals of $Cu_{2-x}Se$ have been prepared via various routes, including colloidal synthesis methods in hot surfactants.[4] In contrast, CuSe has a hexagonal phase at room temperature, and it is often found as impurity in copper(I) selenide.[5]

We report the synthesis of colloidal $Cu_{2-x}Se$ nanocrystals using noncoordinating 1-octadecene (ODE) as solvent and oleylamine as both the reductant for Se (converting it to Se^{2-}) and the ligand for the nanocrystals, thus avoiding the use of toxic, pyrophoric, and expensive alkylphosphines. Anhydrous CuCl (0.099 g, 1 mmol), which is known to be stable source of Cu(I),[6] was added to a mixture of 5 mL of oleylamine and 5 mL of ODE in a flask. After the system was pumped to vacuum for 1 h at 80 °C using a Schlenk line, the mixture was put under nitrogen flow. Next, the temperature was increased to 300−310 °C, and a suspension of Se (0.039 g, 0.5 mmol) in 1 mL of ODE was quickly injected using a syringe. The temperature was allowed to rise to the preinjection value. The total reaction time after injection was 15 min, after which the flask was cooled rapidly to room temperature and 5 mL of toluene was added to it. The mixture was transferred to a glovebox and cleaned 2−3 times by precipitation with ethanol. The nanocrystals were then redispersed in toluene or trichloroethylene. The sample also contained a small amount of hexagonal platelets, often larger than 100 nm, made of hexagonal CuSe,[7] which could be precipitated by centrifugation (see Figure 3a,b). The much smaller particles left in solution (Figure 1) had mainly cuboctahedral shapes, and most of them had a cubic structure. Distinctive sets of lattice fringes were identified using high-resolution transmission electron microscopy (HRTEM), including ones corresponding to the (111) and (220) reticular planes of $Cu_{2-x}Se$ ($d_{111}^{Cu_{2-x}Se} = 3.36$ Å and $d_{220}^{Cu_{2-x}Se} = 2.06$ Å), but some particles had hexagonal structure (hcp CuSe).[7]

The average composition, determined by energy-dispersive X-ray spectroscopy (EDS), ranged from $Cu_{1.70}Se$ to $Cu_{1.90}Se$, depending on the synthesis.[7] Since ∼5% of the nanocrystals were hexagonal CuSe, the composition of the cubic $Cu_{2-x}Se$ nanocrystals ranged from $Cu_{1.68}Se$ to $Cu_{1.80}Se$.

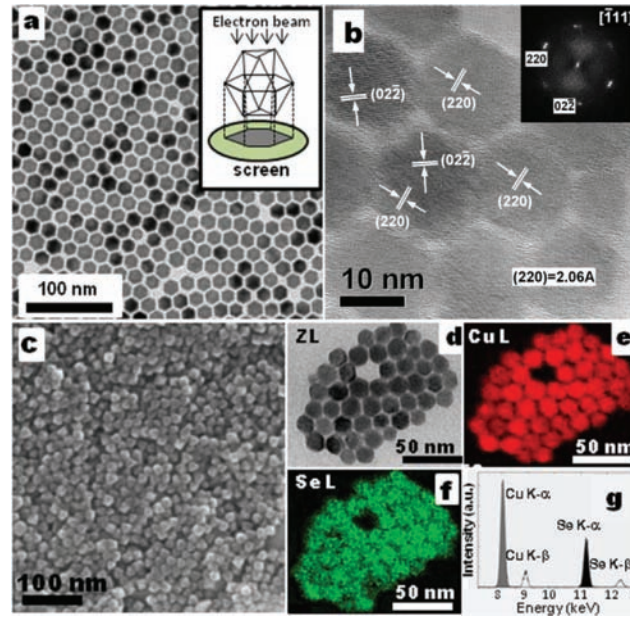

Figure 1. (a) TEM image of size-selected $Cu_{2-x}Se$ nanocrystals grown for 15 min at 300 °C, having an average size of 16 nm (the size estimated by XRD was 18 nm). The inset shows a sketch of the hexagonal projection of a cuboctahedron shape. (b) HRTEM image of $Cu_{2-x}Se$ nanocrystals. Most of the displayed nanocrystals are seen under their [1̄11] zone axis. The inset shows their two-dimensional fast Fourier transform. (c) Scanning electron microscopy image of $Cu_{2-x}Se$ nanocrystals drop-casted from solution onto a glass substrate. (d) Elastic-filtered (ZL) image of several nanocrystals. (e, f) Cu and Se elemental maps from the same group obtained by filtering the Cu L edge (at 931 eV) and the Se L edge (at 1436 eV). (g) Elemental quantification of a group of nanocrystals by EDS.

Elemental mapping via energy-filtered TEM (using the three-windows method)[8] confirmed that both Cu and Se were uniformly distributed among the nanocrystals, which means that there was no appreciable compositional variation among them (Figure 1d−f) except for the occasional presence of the CuSe nanocrystals. Control syntheses with no oleylamine yielded CuCl and elemental Se, while the absence of ODE led to the formation of polydisperse nanocrystals with mixed phases. The powder X-ray diffraction (XRD) patterns of the as-synthesized $Cu_{2-x}Se$ nanocrystals could be fitted according to one form of the berzelianite Cu_2Se phase (Figure 2). Indeed, the (111)/(220) peak intensity ratio was higher than expected

[†] Istituto Italiano di Tecnologia.
[‡] CNR-Istituto di Crystallografia.

10.1021/ja103223x

for the bulk structure. This effect could be explained by considering a deviation in the occupancies of the Cu ions from those of the bulk, as proved by Rietveld analysis of the XRD patterns, which fitted well to the α-$Cu_{1.8}Se$ phase.[7] Often two additional peaks (with much lower intensity) appeared at $2\theta = 25.35$ and 28.07° and were assigned to hexagonal CuSe. On the basis of the XRD data, the approximate weight percentage of CuSe nanoparticles in the sample was ~5%.[9] Figure 2b−d presents X-ray photoelectron spectroscopy (XPS) data for the as-synthesized nanocrystals. The binding energies were 932.30 eV for Cu $2p_{3/2}$ and 54.84 eV for Se 3d in $Cu_{2-x}Se$.[4a] The Cu 2p peak had a satellite line at 940−945 eV due to Cu(II) (likely CuSe). A small peak at 58−60 eV pointed to a high oxidation state of Se (possibly SeO_2).

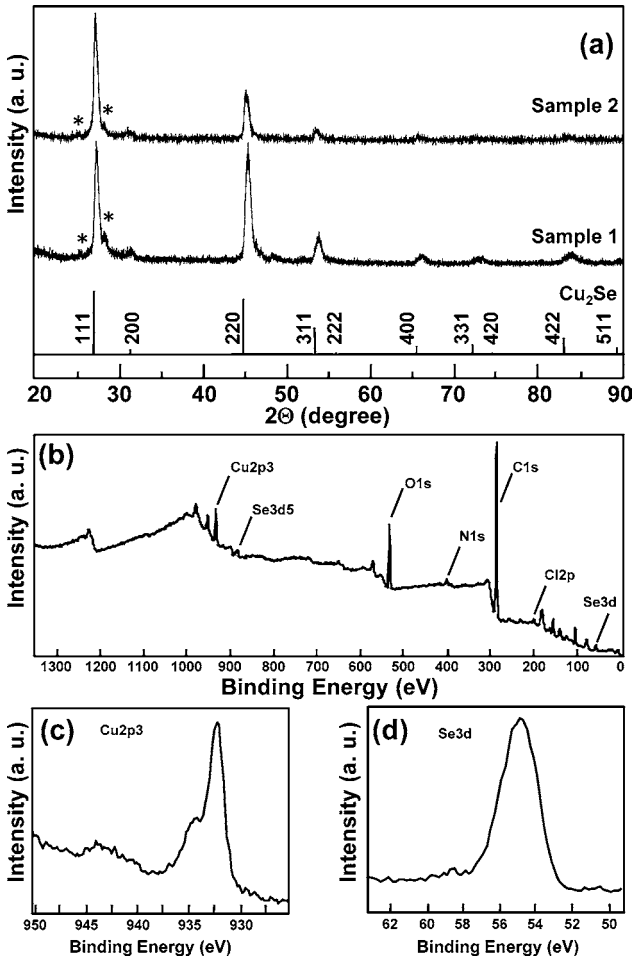

Figure 2. (a) XRD patterns of two different $Cu_{2-x}Se$ samples along with the bulk XRD pattern of cubic Cu_2Se. Peaks marked as * refer to hexagonal CuSe. (b) XPS survey spectrum of one sample: C, O, Cl, and N (from oleylamine) along with Cu and Se are present. XPS core-level spectra of $Cu_{2-x}Se$ from (c) Cu 2p3 and (d) Se 3d. The binding energies found using XPS were corrected for specimen charging by referencing the C 1s line to 284.81 eV.

In the present system, in addition to the specific choice of surfactants, the reaction temperature was also critical in phase control: syntheses performed at temperatures ≥315 °C yielded a mixture of tetragonal (mainly Cu_2Se) nanocrystals and metallic Cu nanoparticles (Figure 3) with various shapes,[7,10] and their overall size distribution was broader than that of the nanoparticles synthesized at lower temperature. Furthermore, these nanocrystals were often aggregated. The formation of metallic Cu in these cases can be explained by the competitive reduction of Cu(I) by oleylamine at higher temperatures, as confirmed by test syntheses.[7] The formation of other phases of $Cu_{2-x}Se$ (mainly tetragonal here; also see the XRD pattern in the Supporting Information) deserves further discussion. $Cu_{2-x}Se$ can crystallize in a large number of phases, often with small differences in energy of formation among them, and in each of these phases, copper can be found in a range of stoichiometries. In the bulk, the tetragonal phase of $Cu_{2-x}Se$ is stable up to 413 K, above which the cubic phase is more stable.[11] This is different from what we found for the nanocrystals. Many studies have reported syntheses of $Cu_{2-x}Se$ nanoparticles with mixed phases, and this is not surprising in nanocrystals, for which the contribution of the surface energy to the total energy of formation is not negligible and the growth rates of various facets can be influenced strongly by the reaction environment. Therefore, slightly different growth conditions (even just a different choice in the surfactants or a different reaction temperature) can favor the growth of one phase over others. In the present case, for example, there appears to be a window of experimental conditions that promotes the formation of the "metastable" tetragonal phase of copper selenide.

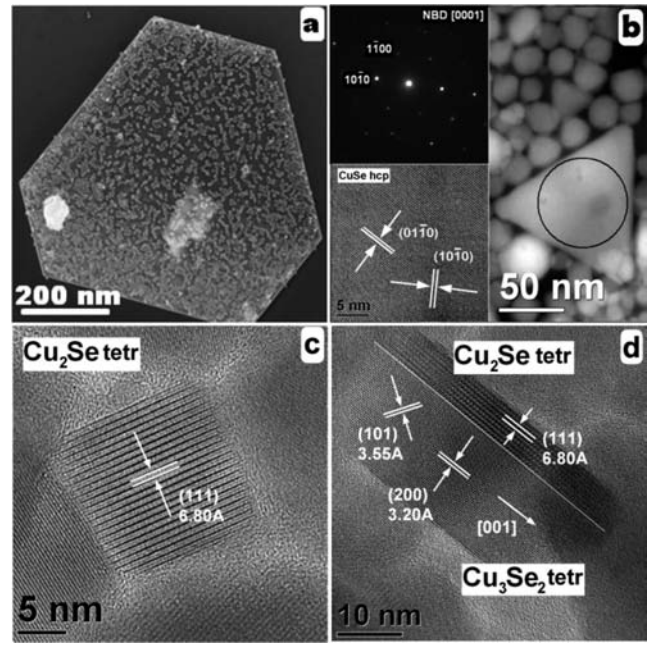

Figure 3. (a) Field-emission scanning electron microscopy (FESEM) image of a CuSe hexagonal platelet with small nanocrystals lying on its top facet. (b) High-angle annular dark-field scanning TEM (HAADF-STEM) image of a CuSe triangular platelet. The insets display the corresponding nano beam diffraction (NBD) and HRTEM image of the platelet and demonstrate that it is made of hcp CuSe (space group $P6_3/mmc$) observed along the [0001] zone axis. In the HRTEM image, the $(10\bar{1}0)$ and $(01\bar{1}0)$ lattice planes (interplanar distance 3.41 Å) can be seen. The black circle on the platelet corresponds to the NBD area. (c) HRTEM image of Cu_2Se nanocrystals having a tetragonal phase (space group $P4_2/n$). The (111) lattice planes (reticular distance 6.80 Å) are visible. (d) HRTEM image of a nanocrystal formed by two domains having different tetragonal phases and epitaxially connected to each other. One domain has a Cu_3Se_2 phase (space group $P4_21m$). The domain is observed along the [010] zone axis and shows the (101) and (200) lattice planes (interplanar distances 3.55 and 3.20 Å, respectively). The other domain has instead a Cu_2Se phase (space group $P4_2/n$) and shows the (111) lattice planes.

Typical optical absorption spectra of $Cu_{2-x}Se$ nanocrystals dissolved in trichloroethylene and deposited as dense films on glass substrates are shown in Figure 4a. In solution, a first absorption shoulder was seen at 480 nm (2.58 eV), which is blue-shifted with respect to the direct band gap of bulk copper selenide (2.4 eV).

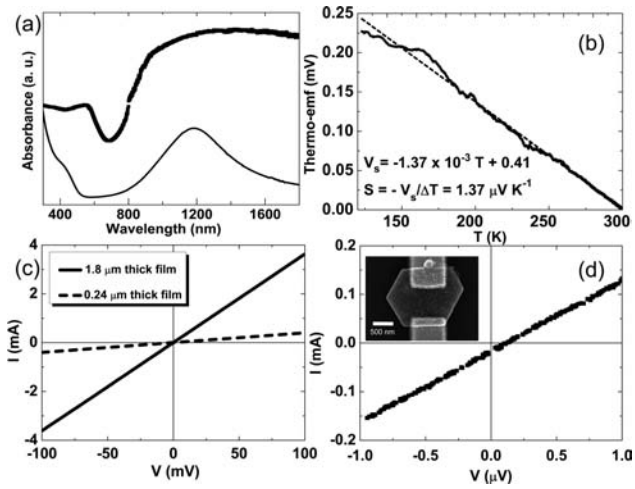

Figure 4. (a) Optical absorption spectra of $Cu_{2-x}Se$ nanocrystals dispersed in trichloroethylene (solid line) and of a film of $Cu_{2-x}Se$ nanocrystals on glass protected from oxidation by PMMA coverage (squares). (b) Plot of thermoelectromotive force (thermo-emf) voltage vs cold probe temperature. The top and bottom inset formulas indicate the fitting equation of the data and the calculation of the thermal power (S),[15] respectively. (c) Current−voltage ($I-V$) curves of two films of different thicknesses prepared by drop-casting from the same sample of $Cu_{2-x}Se$ nanocrystals. The curves were recorded under ambient conditions using silver paste to form the contact pads between the probes and the film. We obtained resistivities of 5.76×10^{-3} and 6.56×10^{-3} Ω cm for the films with thicknesses of 1.8 and 0.24 μm, respectively. (d) $I-V$ data recorded from a single CuSe platelet that was contacted by electrodes fabricated by electron-beam lithography and metal evaporation of chromium (5 nm) and gold (100 nm). The derived sheet resistance of a platelet was $\sim 1 \times 10^{-5}$ Ω cm. The inset shows a scanning electron microscopy image of a hexagonal-shaped CuSe platelet contacted by two metal electrodes. All of the reported current transport experiments were performed under ambient conditions.

The direct-band-gap transition is more pronounced in the spectra recorded from $Cu_{2-x}Se$ films and is red-shifted by 0.30 eV with respect to the solution case as a result of superlattice effects arising from the dense nanocrystal packing in the film.[7] A broad and intense absorption peak was observed at 1150 nm (in solution), which is attributed to transitions involving the indirect band gap. We investigated the conductive properties of films of $Cu_{2-x}Se$ nanocrystals of various thicknesses that were prepared by drop-casting nanocrystal solutions onto glass substrates inside the glovebox. Thermoelectric measurements were performed to determine the majority carrier type in the films (Figure 4b). The polarity of the thermoelectromotive force was positive, implying p-type semiconducting behavior,[13] which can be attributed to the acceptor levels created by copper ions during the formation of copper-deficient nanocrystals. In the current-voltage measurements we found film resistivities of $\sim 6 \times 10^{-3}$ Ω cm (see Figure 4c), in good agreement with the data reported in ref 12. Such low resistivities may suggest the use of $Cu_{2-x}Se$ nanocrystals as hole-injection layers in optoelectronic devices.[14] We did not observe any significant difference between the conductance of films that were covered by poly(methyl methacrylate) (PMMA) to prevent oxidation of the nanocrystals and that of bare, unprotected films. Also, the nanocrystal films were slightly contaminated by the CuSe platelets in these experiments (no size-selective precipitation had been carried out on these samples). We measured the current−voltage characteristics of individual CuSe platelets, as shown in Figure 4d, and derived for these platelets a film resistivity that is 3 orders of magnitude smaller than those of the nanocrystal films. This result is reasonable, since within a platelet the charge transport is not hindered by the potential barrier of the surfactants, as it is the case of the nanocrystal film. However, we do not expect isolated CuSe platelets to have a significant impact on the film resistance.

In conclusion, we have synthesized $Cu_{2-x}Se$ nanocrystals using a colloidal approach that avoids the use of phosphines. The nanocrystals show a distinct optical absorption shoulder in the UV and a peak in the NIR region with a high absorption coefficient. Thermoelectric measurements on films of nanocrystals confirmed p-type conductivity, hence making them potential candidates for use in solid-state solar cells.

Acknowledgment. We thank Mauro Povia, Eloisa Sardella, Sergio Marras, and Andrea Falqui for help with XRD, XPS, and HRTEM measurements. Financial support via the FP7 Starting ERC Grant NANO-ARCH (Contract 240111) is acknowledged.

Supporting Information Available: Chemicals, experimental details, control reactions, EDX and HRTEM images, XRD refinements, additional XRD patterns, and optical absorption spectra. This material is available free of charge via the Internet at http://pubs.acs.org.

References

(1) (a) Goetzberger, A.; Hebling, C.; Schock, H. W. *Mater. Sci. Eng., R* **2003**, *40*, 1. (b) Kamat, P. V. *J. Phys. Chem. C* **2008**, *112*, 18737. (c) Wadia, C.; Alivisatos, A. P.; Kammen, D. M. *Environ. Sci. Technol.* **2009**, *43*, 2072. (d) Holder, E.; Tessler, N.; Rogach, A. L. *J. Mater. Chem.* **2008**, *18*, 1064. (e) Hillhouse, H. W.; Beard, M. C. *Curr. Opin. Colloid Interface Sci.* **2009**, *14*, 245. (f) Talapin, D. V.; Lee, J. S.; Kovalenko, M. V.; Shevchenko, E. V. *Chem. Rev.* **2010**, *110*, 389.
(2) (a) Rockett, A.; Birkmire, R. W. *J. Appl. Phys.* **1991**, *70*, R81. (b) Hu, Y. X.; Afzaal, M.; Malik, M. A.; O'Brien, P. *J. Cryst. Growth* **2006**, *297*, 61. (c) Lin, F.; Bian, G. Q.; Lei, Z. X.; Lu, Z. J.; Dai, J. *Solid State Sci.* **2009**, *11*, 972.
(3) (a) Siebentritt, S. *Thin Solid Films* **2002**, *403*, 1. (b) Guo, Q. J.; Hillhouse, H. W.; Agrawal, R. *J. Am. Chem. Soc.* **2009**, *131*, 11672. (c) Steinhagen, C.; Panthani, M. G.; Akhavan, V.; Goodfellow, B.; Koo, B.; Korgel, B. A. *J. Am. Chem. Soc.* **2009**, *131*, 12554. (d) Arici, E.; Sariciftci, N. S.; Meissner, D. *Adv. Funct. Mater.* **2003**, *13*, 165.
(4) (a) Wang, W. Z.; Yan, P.; Liu, F. Y.; Xie, Y.; Geng, Y.; Qian, Y. T. *J. Mater. Chem.* **1998**, *8*, 2321. (b) Xie, Y.; Zheng, X. W.; Jiang, X. C.; Lu, J.; Zhu, L. Y. *Inorg. Chem.* **2002**, *41*, 387. (c) Zhang, A. Y.; Ma, Q.; Lu, M. K.; Zhou, G. J.; Li, C. Z.; Wang, Z. G. *J. Phys. Chem. C* **2009**, *113*, 15492. (d) Zhu, J. J.; Palchik, O.; Chen, S. G.; Gedanken, A. *J. Phys. Chem. B* **2000**, *104*, 7344. (e) Ingole, P. P.; Joshi, P. M.; Haram, S. K. *Colloids Surf., A* **2009**, *337*, 136.
(5) Wei, W.; Zhang, S. Y.; Fang, C. X.; Zhao, S. Q.; Jin, B. K.; Wu, J. Y.; Tian, Y. P. *Solid State Sci.* **2008**, *10*, 622.
(6) Malik, M. A.; O'Brien, P.; Revaprasadu, N. *Adv. Mater.* **1999**, *11*, 1441.
(7) See the Supporting Information for additional details.
(8) Egerton, R. F. *Electron Energy Loss Spectroscopy in the Electron Microscope*, 2nd ed.; Plenum Press: New York, 1996.
(9) We used PowderCell (http://www.ccp14.ac.uk).
(10) Haram, S. K.; Santhanam, K. S. V.; Neumannspallart, M.; Levyclement, C. *Mater. Res. Bull.* **1992**, *27*, 1185.
(11) Kashidaa, S.; Shimosakab, W.; Moric, M.; Yoshimura, D. *J. Phys. Chem. Solids* **2003**, *64*, 2357.
(12) Bhuse, V. M.; Hankare, P. P.; Garadkar, K. M.; Khomane, A. S. *Mater. Chem. Phys.* **2003**, *80*, 82.
(13) Mane, R. S.; Kajve, S. P.; Lokhande, C. D.; Han, S. H. *Vacuum* **2006**, *80*, 631.
(14) Hiramatsu, H.; Koizumi, I.; Kim, K. B.; Yanagi, H.; Kamiya, T.; Hirano, M.; Matsunami, N.; Hosono, H. *J. Appl. Phys.* **2008**, *104*, 11.
(15) Taylor, P. L. *Phys. Rev. B* **1973**, *7*, 1197.

JA103223X